Parametric resonance in a conservative system of coupled nonlinear oscillators

Johann Maddi, Christophe Coste, Michel Saint-Jean

Parametric resonance in a conservative system of coupled nonlinear oscillators.

Johann Maddi, Christophe Coste, and Michel Saint Jean

Laboratoire "Matière et Systèmes Complexes" (MSC), UMR 7057 CNRS,

Université Paris–Diderot (Paris 7), 75205 Paris Cedex 13, France

(Dated: May 13, 2022)

Abstract

We study a dimer in a periodic potential well, which is a conservative but non integrable system. This seemingly simple system exhibits a surprisingly rich dynamics. Using a systematic asymptotic analysis, we demonstrate that the translation mode of the dimer (center of mass motion) may induce a parametric resonance of the oscillatory mode. No external forcing occurs, thus this system belongs to the class of autoparametric systems. When the dimer energy is such that both particles are trapped in neighboring potential wells, we derive the relevant amplitude equations for the eigenmodes (center of mass motion and relative motion) and show that they are integrable. In the opposite limit, when the dimer slides along the external potential so that the center of mass motion is basically a translation, we also exhibit autoparametric amplification of the relative motion. In both cases our calculations provide reliable estimates of the relevant parameters for the autoparametric resonance to appear. Moreover, the comparison between the numerical integration of the actual system and the asymptotic analysis evidences an excellent quantitative agreement.

I. INTRODUCTION

The dynamics of coupled linear oscillators is easily described as a superposition of their eigenmodes motions. This is not the case for nonlinear oscillators, since their characteristic frequencies depend on the amplitude of the oscillations. The coupling may therefore induce a resonant response of some of the oscillatory modes. Nonlinear resonances are very common in physical systems, and usually difficult to analyse [1].

When energy is supplied by an external source, in such a way that a characteristic parameter of the oscillator becomes time-dependant, such as *e.g.* the length of a pendulum, the oscillator response may exhibit parametric resonance [2]. A paradigm of the parametric resonance is the nonlinear Mathieu equation [3–8]. The resonance phenomenon is maximized when the forcing frequency ω is roughly twice the natural frequency ω_0 of the oscillator, more precisely in a *resonance tongue* centered on $\omega = 2\omega_0$, with a width that depends on the forcing amplitude. When this frequency tuning happens, a typical feature of parametric resonance is the very slow increase of the parametrically amplified oscillatory mode. There are thus two time scales, a fast one which is the frequency of the forcing and a slow one which characterises the slowly varying amplitude of the forced oscillator. The nonlinear Mathieu equation is not a conservative system, but when dissipation is not taken into account, the amplitude equation [5] that describes the slow dynamics is conservative. Physically, it means that the energy transfer between the oscillator and the external source that provides the parametric excitation vanishes when averaged on the slow time scale.

In a conservative system, without any external source, there could be a resonant energy exchange between two oscillatory modes. Recent studies have considered coupled Duffing oscillators [9–12] that exhibit nonlinear resonant response. A swinging spring is another well known mechanical apparatus that may evidence resonant behavior when the frequencies of the elastic and pendular oscillations are in the ratio 2:1 [13, 14]. In astronomy, quasi-periodic oscillations (QPO) are observed in accretion disks of massive neutron stars or black holes, and it has been suggested that the QPOs arise from the coupling of two oscillatory modes [15–18]. A particle in the accretion disk may have radial, vertical and azimuthal epicyclic oscillations around its stable orbit, and because of angular momentum conservation only two of them are independent, and may exhibit a resonance [17]. Such resonances are called *autoparametric* because there is no external forcing, and the behavior of the resonant mode mimics two

well known characteristics of parametric resonance. The amplitude of the resonant mode is a function of time that exhibits an initial exponential increase, and that evolves with a characteristic timescale much larger than the period of the forcing oscillations.

In this paper, we consider a nonlinear conservative system with two degrees of freedom. More precisely, we study a dimer, made of two interacting point particles submitted to an external periodic potential and moving on a line. Such a system is in some sense a toy model of an adatoms cluster moving on a surface [19–21]. This seemingly simple system exhibits a surprisingly rich dynamics, as shown in an heuristic way in Ref. [20] in which an autoparametric resonance of the dimer was observed. We proceed to a systematic asymptotic expansion of the equations of motion when a small parameter $|\epsilon| \ll 1$ may be defined, taking into account in a consistent fashion the nonlinearities of the interaction and confining potential. This multiscale analysis [22] is not only a convenient technical tool, but it also provides relevant orders of magnitude. When the dimer remains trapped in a well of the external potential, assuming a ratio of the dimer energy on the confining potential of order ϵ^2, an autoparametric resonance of the dimer vibrations is seen if the interaction potential stiffness is of order ϵ^2, the slow timescale that characterises the parametric amplification is found order ϵ^{-2} and the width of the resonance tongue is of order ϵ. In the opposite limit such that the initial kinetic energy is high enough for the dimer center of mass to slide on the external potential, if ϵ is the order of magnitude of the vibrations, the sliding velocity is of order ϵ^0, and an autoparametric resonance of the vibrations is observed if the the interaction potential stiffness is of order ϵ^0, with a characteristic resonance time of order ϵ^{-2} and a width of the resonance tongue that is of order ϵ^2.

The theoretical analysis of the dimer motions is done in Section II. This theoretical analysis is completed by two appendices devoted to technical details. In Section III, we compare our perturbative solution to a numerical integration of the actual equations of the motions for a dimer in a periodic external potential. When the initial conditions are such that the relevant conditions for the validity of the perturbative analysis are fulfilled, an excellent agreement between the actual motion and our theoretical description is evidenced. In Section IV we sum up our conclusions.

II. DIMER IN A PERIODIC POTENTIAL : AMPLITUDE EQUATIONS.

The dimer is made of two point particles of mass m that interact with a potential $U_{int}(r)$ where r is the distance between the particles, submitted to an external periodic potential and moving on a line. We take a sinusoïdal external potential of period a,

$$U_{ext}(x_1, x_2) = U_0 \left(2 - \cos \frac{2\pi x_1}{a} - \cos \frac{2\pi x_2}{a} \right), \tag{1}$$

where x_i is the spatial coordinate of the i-th particle ($i = 1, 2$) and $2U_0$ is the potential barrier per particle. We consider the commensurate configuration for which the period a is also the dimer equilibrium length. Setting $\ddot{x}_i \equiv \mathrm{d}^2 x_i / \mathrm{d}t^2$, the equations of motion are

$$\begin{cases} m\ddot{x}_1 = -\partial U_{int}/\partial x_1 - (2\pi U_0/a) \sin(2\pi x_1/a), \\ m\ddot{x}_2 = -\partial U_{int}/\partial x_2 - (2\pi U_0/a) \sin(2\pi x_2/a), \end{cases} \tag{2}$$

There are two configurations in which this system may be solved perturbatively. In the first case, the dimer particles are trapped in adjacent external potential wells, and the small parameter depends on the ratio $E_0/U_0 \ll 1$ where E_0 is the initial energy of the dimer. This configuration is studied in Sec. II A. The second case is, in some sense, the opposite limit when the center of mass slides along the external potential. In this case, the small parameter depends on the ratio $U_0/(mV_0^2) \ll 1$, where V_0 is the mean velocity of the center of mass. This configuration is studied in Sec. II B.

A. Dimer in a well.

Let us first assume that the dimer, during its motion, does not escape the external potential well. Because of the commensurability assumption, when both particles are in adjacent wells of the external potential the interaction potential is also minimum. It is sufficient to take its harmonic approximation with a stiffness k, so that the equations of motion read

$$\begin{cases} m\ddot{x}_1 = k(x_2 - x_1 - a) - (2\pi U_0/a) \sin(2\pi x_1/a), \\ m\ddot{x}_2 = k(x_1 - x_2 + a) - (2\pi U_0/a) \sin(2\pi x_2/a). \end{cases} \tag{3}$$

We rescale the variables using $a/(2\pi)$ as the unit length, U_0 as the unit energy and therefore $\sqrt{ma^2/(4\pi^2 U_0)}$ as the unit time. Moreover, we introduce the normal modes as

$$x \equiv \frac{x_1 + x_2}{2} - \pi, \quad y \equiv \frac{x_2 - x_1}{2} - \pi, \tag{4}$$

in dimensionless units. The mode x is the center of mass motion, and the mode y the relative motion of the dimer particles. The potential energy reads

$$U(x, y) = 2\left(1 - \cos x \cos y + K y^2\right), \tag{5}$$

where $K = ka^2/(4\pi^2 U_0)$ is the dimensionless stiffness. The equations of motion become

$$\begin{cases} \ddot{x} &= -\sin x \cos y, \\ \ddot{y} &= -2Ky - \cos x \sin y. \end{cases} \tag{6}$$

This set of equations provides an exact description of the dimer motions, since it amounts to a rewriting of Eqn. (3) with the new variables (4). The configuration of a trapped dimer in adjacent potential wells corresponds to the equilibrium position $x = 0(\mathrm{mod}\pi)$ and $y = 0$.

We search for a solution of the system (6) perturbatively, using the method of multiple scales. We introduce a small parameter ϵ, with $|\epsilon| \ll 1$ and let $x = \mathcal{O}(\epsilon)$ and $y = \mathcal{O}(\epsilon)$, and we introduce successive times scales $T_0 = t, T_2 = \epsilon^2 t, \ldots$. Formally, we write

$$\begin{cases} x(t) = \epsilon X_1(T_0, T_2, \ldots) + \epsilon^3 X_3(T_0, T_2, \ldots) + \ldots, \\ y(t) = \epsilon Y_1(T_0, T_2, \ldots) + \epsilon^3 Y_3(T_0, T_2, \ldots) + \ldots, \\ \dfrac{\mathrm{d}^2}{\mathrm{d}t^2} = \dfrac{\partial^2}{\partial T_0^2} + 2\epsilon^2 \dfrac{\partial^2}{\partial T_0 \partial T_2} + \ldots. \end{cases} \tag{7}$$

Up to order ϵ^3, the equations of motion are given by the system :

$$\begin{cases} \ddot{x} &= -x + \dfrac{1}{2} y^2 x + \dfrac{1}{6} x^3, \\ \ddot{y} &= -(2K+1) y + \dfrac{1}{6} y^3 + \dfrac{1}{2} y x^2. \end{cases} \tag{8}$$

All nonlinear terms are of order ϵ^3, therefore a necessary condition for a parametric resonance to appear is a very small stiffness of the dimer interaction, such that $K = \mathcal{O}(\epsilon^2)$. To this end, we set $K \equiv \epsilon^2 \widetilde{K}$ where $\widetilde{K}$ is assumed to be of order ϵ^0, so that the nonlinearities are of the same order of magnitude as the detuning between the two oscillatory modes. Our

calculations will validate *a posteriori* this ansatz, because $\widetilde{K}$ will indeed be found to give the width of the resonance tongue.

At order $\mathcal{O}(\epsilon)$, the two modes $X_1(T_0)$ and $Y_1(T_0)$ behave as free uncoupled harmonic oscillators with the same frequency (1 in our dimensionless variables) so that the solutions at this order are

$$X_1 = A(T_2)e^{iT_0} + \overline{A}(T_2)e^{-iT_0}, \quad Y_1 = B(T_2)e^{iT_0} + \overline{B}(T_2)e^{-iT_0}, \tag{9}$$

where $A(T_2)$ and $B(T_2)$ are slowly varying complex amplitudes.

The multiple scales method is particularly simple to apply in the present case, because at order ϵ^3, the equations for $X_3(T_0)$ and $Y_3(T_0)$ are both that of a forced harmonic oscillator. Since this method is well described in textbooks [22] we do not give the details of the calculations. To ensure the consistency of the asymptotic expansion, one requires the vanishing of the *secular terms* which would induce a forcing at the characteristic oscillator frequency of X_3 and Y_3. The relevant amplitude equations, which give the evolution of the oscillator amplitude with the slow time-scale are obtained when these secular terms are eliminated. This solvability condition provides the following coupled amplitude equations :

$$\begin{cases} 2i\dfrac{\partial A}{\partial T_2} = \dfrac{1}{2}|A|^2A + |B|^2A + \dfrac{1}{2}B^2\overline{A}, & \text{(a)} \\ 2i\dfrac{\partial B}{\partial T_2} = -2\widetilde{K}B + \dfrac{1}{2}|B|^2B + |A|^2B + \dfrac{1}{2}A^2\overline{B}. & \text{(b)} \end{cases} \tag{10}$$

We will see that these amplitude equations are an integrable dynamical system. Before providing a complete phase portrait of the system (10), lets us begin by its simplest equilibrium solutions. An obvious equilibrium is $(A = 0, B = 0)$, which is marginally stable since the frequency for A vanishes. This solution is basically worthless and reflects the stable equilibrium position of the dimer in the potential well.

In contrast, the solution $(A_0 \neq 0, B = 0)$, with $4i(\partial A_0/\partial T_2) = |A_0|^2A_0$ is of great physical significance. Setting $A_0 \equiv a_0e^{i\phi_0}$, and separating real and imaginary parts, we get $A_0(T_2) = a_0 \exp -i\,(a_0^2T_2/4 + \phi_0)$, where a_0 and ϕ_0 do not depend on T_2. The center of mass motion is thus

$$x(t) = 2\epsilon a_0 \cos\left[\left(1 - \frac{\epsilon^2 a_0^2}{4}\right)t + \phi_0\right], \tag{11}$$

which exhibits an amplitude dependent frequency (Borda frequency) because of the nonlin-

earities. When this solution for A is injected into the equation for B, we get

$$2i\frac{\partial B}{\partial T_2} = -2\widetilde{K}B + \frac{1}{2}|B|^2B + a_0^2B + \frac{a_0^2}{2}e^{-ia_0^2T_2/2}\overline{B},$$

where we have chosen $\phi_0 = 0$. Setting $B(T_2) = D(T_2)\exp(-ia_0^2T_2/4)$, we get the autonomous equation

$$\frac{\partial D}{\partial T_2} = i\left(\widetilde{K} - \frac{a_0^2}{4}\right)D + i\frac{a_0^2}{4}\overline{D} - \frac{i}{4}|D|^2D. \tag{12}$$

The dynamics of the amplitude D is thus given by the normal form [23] of the amplitude equation for a parametrically forced oscillator with a cubic nonlinearity [4, 5, 7]. Moreover, since the coupling terms between A and B are at least quadratic in B in Eqn. (10) (a), the solution for A_0 is linearly stable. The normal form (12) is the only equation relevant to the linear stability analysis of the solution $(A_0, B = 0)$. This solution is thus parametrically unstable for $0 \leqslant \widetilde{K} \leqslant a_0^2/2$ [4, 5, 7]. Physically, it means that the center of mass motion may induce a parametric amplification of the relative motions between the two particles of the dimer. Since there is no external source to induce the parametric resonance, we follow the terminology of Ref. [17] and call this resonant coupling between the two oscillatory modes of the dimer an autoparametric resonance.

There is also a solution $(A = 0, B_0 \neq 0)$, with $4i(\partial B_0/\partial T_2) = -4\widetilde{K}B_0 + |B_0|^2B_0$. Setting $B_0 \equiv b_0e^{i\psi_0}$, we get as before $B(T_2) = b_0\exp -i\left[\left(\widetilde{K} - b_0^2/4\right))T_2 + \psi_0\right]$, where b_0 and ψ_0 do not depend on T_2. To study the linear stability of this solution, let $A = \delta A'$ such that $|\delta A'| \ll 1$. We get from (10) (a)

$$2i\frac{\partial \delta A'}{\partial T_2} = \frac{b_0^2}{4}\delta A' + \frac{ab_0^2}{2}e^{2i\psi}\overline{\delta A'}.$$

We obtain an autonomous equation by setting $\delta A' = \delta Ae^{i\psi}$,

$$i\frac{\partial \delta A}{\partial T_2} = \left(\widetilde{K} + \frac{b_0^2}{4}\right)\delta A + \frac{b_0^2}{4}\overline{\delta A}.$$

If we write $\delta A = \delta A_r + i\delta A_i$, separating real and imaginary part we get that both variables behaves as harmonic oscillators of real frequency

$$\sigma^2 = \widetilde{K}\left(\frac{b_0^2}{2} + \widetilde{K}\right) \geqslant 0,$$

which indicates that this solution is always stable. There is therefore no parametric amplification of the center of mass motion by the relative motion of the particles in the dimer.

We will now fully describe the solutions of the amplitude equations (10), recovering our previous results as special cases. Let us express the complex amplitudes A and B as

$$A(T_2) = a(T_2)e^{i\phi(T_2)}, \quad B(T_2) = b(T_2)e^{i\psi(T_2)}, \tag{13}$$

where the real functions a and b are the amplitudes, and where the real functions ϕ et ψ are the phases. Taking real and imaginary parts in both equations of the system (10), one gets

$$\begin{cases} \dot{a} = \dfrac{b^2 a}{4}\sin\theta, \\ \dot{b} = -\dfrac{a^2 b}{4}\sin\theta, \\ \dot{\theta} = 2\widetilde{K} + \dfrac{1}{2}\left(b^2 - a^2\right)(1+\cos\theta), \end{cases} \tag{14}$$

where for simplicity $\dot{a} \equiv \partial a/\partial T_2$, and the same for $\dot{b}$. We notice that the phase space of the dynamical system is actually of dimension 3, since the phases are involved only through their difference $\theta \equiv 2(\psi - \phi)$. Indeed, the knowledge of the three functions a, b and θ is sufficient to get all dynamical variables since

$$\phi(t) = -\int_0^t \left[\frac{a(u)^2}{4} + \frac{b(u)^2}{2} + \frac{b(u)^2}{4}\cos\theta(u)\right]\mathrm{d}u, \qquad \psi(t) = \phi(t) + \theta(t)/2. \tag{15}$$

In order to get a full phase portrait of our system, it is convenient to search for constants of the motion for the system (14). There is an obvious one,

$$a^2 + b^2 \equiv N \Longleftrightarrow a\mathrm{d}a = -b\mathrm{d}b. \tag{16}$$

There is a second independent constant which may be found as in Ref. [17]. Let us consider θ as a function of a, so that

$$\dot{\theta} = \frac{\mathrm{d}\theta}{\mathrm{d}a}\dot{a} = \frac{b^2 a}{4}\sin\theta\frac{\mathrm{d}\theta}{\mathrm{d}a},$$

where we used the first equation of (14). Injecting this result in the equation for $\dot{\theta}$, and multiplying all terms by $a\mathrm{d}a$, we get

$$\begin{aligned} \frac{b^2a^2}{4}\sin\theta\mathrm{d}\theta - \frac{b^2}{2}\cos\theta a\mathrm{d}a + \frac{a^2}{2}\cos\theta a\mathrm{d}a - 2\widetilde{K}a\mathrm{d}a + \frac{a^3}{2}\mathrm{d}a - \frac{b^2}{2}a\mathrm{d}a = 0 \\ -\frac{b^2a^2}{4}\mathrm{d}\left(\cos\theta\right) - \frac{b^2}{2}\cos\theta\mathrm{d}\left(\frac{a^2}{2}\right) - \frac{a^2}{2}\cos\theta\mathrm{d}\left(\frac{b^2}{2}\right) - \widetilde{K}\mathrm{d}\left(a^2\right) + \mathrm{d}\left(\frac{a^4}{8}\right) + \mathrm{d}\left(\frac{b^4}{8}\right) = 0 \end{aligned}$$

where in the second line we used (16). We thus get a second constant of motion,

$$J \equiv \frac{a^4}{8} + \frac{b^4}{8} - \widetilde{K}a^2 - \frac{b^2a^2}{4}\cos\theta, \tag{17}$$

which is obviously independent on the first one. In appendix A, we derive both constants using lagrangian formalism and Noether theorem. Because of these two independent constants of the motion, our system is integrable.

Let us introduce the dynamical variable $\chi(t)$, such that $0 \leqslant \chi \leqslant 1$, as

$$a(t)^2 \equiv N[1-\chi(t)], \quad b(t)^2 = N\chi(t). \tag{18}$$

We show in appendix B that an appropriate definition of the small parameter ϵ allows to take $N = 1$ without any loss in generality, and we will do it henceforward.

Using (14), we get the dynamical equations

$$\begin{cases} \dot{\chi} &= -\dfrac{1}{2}\chi(1-\chi)\sin\theta, \\ \dot{\theta} &= 2\widetilde{K} + \dfrac{1}{2}(2\chi-1)(1+\cos\theta). \end{cases} \tag{19}$$

There is a pair of fixed points

$$\chi^* = 0, \quad \cos\theta^* = 4\widetilde{K} - 1, \tag{20}$$

if we are in the autoparametric (AP; $0 \leqslant \widetilde{K} \leqslant 1/2$) regime. Since the constant of the motion is

$$J(\chi,\theta) = \frac{1}{8} - \frac{1}{4}\chi(1-\chi)(1+\cos\theta) - \widetilde{K}(1-\chi), \tag{21}$$

these fixed points correspond to $J = 1/8 - \widetilde{K}$. Introducing small perturbations $(\delta\chi, \delta\theta)$, the linear stability analysis gives

$$\delta\dot{\chi} = -\frac{1}{2}\sin\theta^*\delta\chi, \quad \delta\dot{\theta} = \sin\theta^*\delta\theta, \tag{22}$$

which shows that these fixed points are saddle points.

The other fixed point is

$$\chi^* = \frac{1}{2} - \widetilde{K}, \quad \theta^* = 0, \tag{23}$$

which only exists in the AP regime, and which corresponds to $J = -\widetilde{K}(1+\widetilde{K})/2$. The linear stability analysis gives

$$\delta\ddot{\chi} = -\left(\frac{1}{2} - \widetilde{K}\right)\left(\frac{1}{2} + \widetilde{K}\right)\delta\chi,$$

showing that this fixed point is a node.

Knowing the constant of motion J, we can plot the phase portrait of the dynamical system in the plane (θ, χ). In the AP regime, J has the local minimum $J = 1/8 - \widetilde{K}$ for the fixed points (20), and the absolute minimum $J = -\widetilde{K}\left(\widetilde{K}+1\right)/2$ for the fixed point (23). Therefore

$$\begin{cases} -\widetilde{K}(\widetilde{K}+1)/2 \leqslant J \leqslant 1/8 \qquad \text{(AP)}, \\ 1/8 - \widetilde{K} \leqslant J \leqslant 1/8 \qquad \text{(NR)}, \end{cases} \tag{24}$$

where NR means non resonant case.

The available range of χ is obtained by taking the square of the equation for $\dot{\chi}$ in (19), expressing the result as a function of $\cos\theta$ and eliminating θ with the help of (17). Indeed, we eventually get

$$4\left(\frac{\mathrm{d}\chi}{\mathrm{d}t}\right)^2 = \chi^2(1-\chi)^2 - \left[\frac{\chi^2+(1-\chi)^2}{2} - 4\widetilde{K}(1-\chi) - 4J\right]^2 \equiv F(\chi)^2 - G(\chi)^2, \tag{25}$$

which shows that the motion is restricted to those values of χ for which the right-hand-side is positive. The solutions of $F(\chi) = +G(\chi)$ are

$$\chi_{\pm}^{+} = \frac{1}{2} - \widetilde{K} \pm \sqrt{\left(\widetilde{K}+\frac{1}{2}\right)^2 - \frac{1}{4} + 2J}. \tag{26}$$

Since $\chi \in [0,1]$ by construction, we must have $\chi_{-}^{+} \geqslant 0$, which implies $J > 1/8 - \widetilde{K}$. Otherwise we must take the solution of $F(\chi) = -G(\chi)$, that reads

$$\chi_{+}^{-} = 1 - \frac{1}{\widetilde{K}}\left(\frac{1}{8} - J\right), \tag{27}$$

Using Eqn. (21), we see that the trajectories in phase space are given by

$$\cos\theta = \frac{\chi^2+(1-\chi)^2 - 8\widetilde{K}(1-\chi) - 8J}{2\chi(1-\chi)} = \frac{G(\chi)}{F(\chi)}, \tag{28}$$

Searching for extremal values of $\cos\theta$, we solve $G'F - F'G = 0$ and get

$$\chi_{\pm}^{*} = 1 - \frac{1-8J}{8\widetilde{K}}\left(1 \pm \sqrt{1 - \frac{8\widetilde{K}}{1-8J}}\right). \tag{29}$$

There are no real solutions in the NR case, which means that $\theta \in [-\pi, \pi]$ for all possible values of J in the NR case, so that only open trajectories occur.

In the AP case, there is a real solution $0 < \chi_{-}^{*} < 1$ for $8\widetilde{K} < 1 - 8J$ (the solution $\chi_{+}^{*} < 0$ has to be rejected). In that case, the trajectories are closed curves, such that $\theta \in [-\theta_{-}^{*}, \theta_{-}^{*}]$

with $\theta_-^* < \pi$. For $\theta = 0$, we deduce from (28) that $F(\chi) = G(\chi)$, so that $\chi(\theta = 0)$ on the closed trajectories is given by $\chi_\pm^+$ in (26). The limit $\chi_-^+ = \chi_+^+$, which requires the vanishing of the square root, is the fixed point (23). These closed trajectories are forbidden for $J \geqslant 1/8 - \widetilde{K}$. The separatrix, between the closed trajectories and the open ones, is thus given by Eqn. (28) for $J = 1/8 - \widetilde{K}$, and therefore includes the two saddle points (20). The linear stability analysis of these points provides the orientation of the separatrix. The orientation of the other trajectories is given by (19), which shows that θ increases with time and that χ increases (decreases) with time for $\theta \in [-\pi, 0]$ ($\theta \in [0, \pi]$).

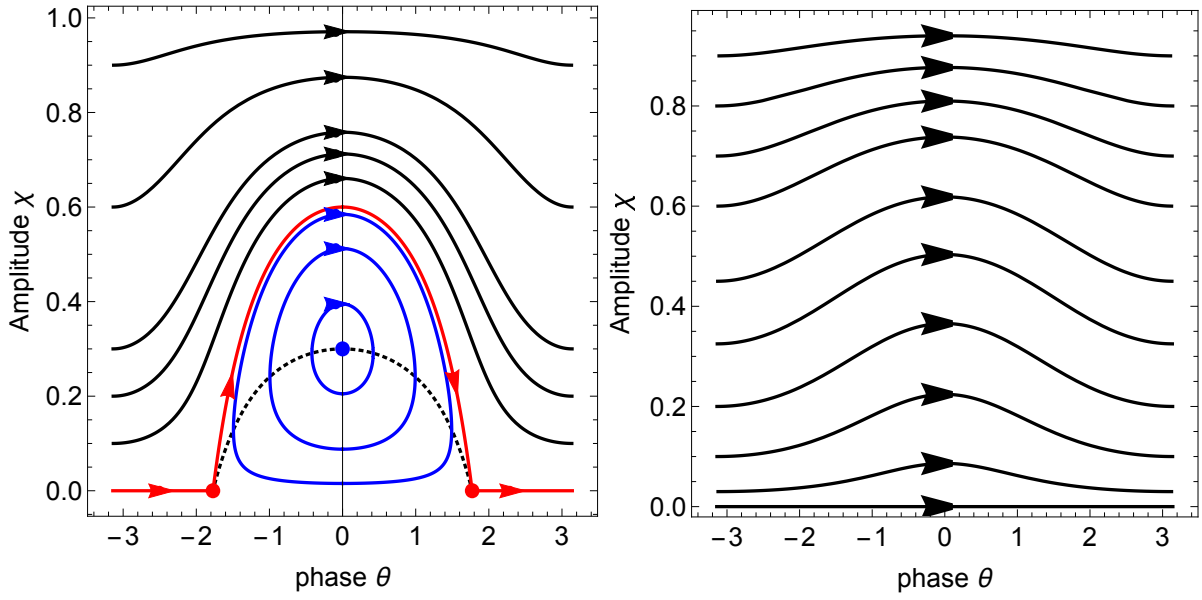

FIG. 1. (Color online) Phase portrait of the dynamical system (14) in the plane (θ, χ). Left plot : AP case, $\widetilde{K} = 0.2$. The separatrix ($J = 1/8 - \widetilde{K}$) is plotted in red, the black dotted line connects the points of vanishing $\dot{\theta}$. The red dots indicate the saddle points on the separatrix, the blue dot indicates the node (23) which corresponds to $J = -\widetilde{K}\left(\widetilde{K}+1\right)/2$. Closed trajectories (blue lines) are observed for $-\widetilde{K}\left(\widetilde{K}+1\right)/2 < J < 1/8 - \widetilde{K}$. Open trajectories (black lines) are observed for $1/8 - \widetilde{K} < J < 1/8$. Right plot, NR case, $\widetilde{K} = 0.7$. All trajectories are open, $1/8 - \widetilde{K} < J < 1/8$.

The phase portraits are shown in Fig. 1, for two values of $\widetilde{K}$. The left plot corresponds to an autoparametric resonance, the right plot to a non resonant case. There is an obvious topological difference between the two phase portraits, since in the left one closed and open trajectories coexist, whereas in the right plot there are only open trajectories.

The left plot provides a fully nonlinear description of the autoparametric resonance, which

completes our previous discussion (12). The key point here is that along the separatrix (solid red line) the relative motion amplitude χ increases from $\chi = 0$ up to a finite maximum amplitude $\chi_{max} = 1 - 2\widetilde{K}$. If one consider any initial condition with a very small amplitude for the relative motion, $0 < \chi_0 \ll 1$, either on an open trajectory or on a closed trajectory, the relevant phase space trajectory will be very close to the separatrix, and the smaller χ_0 the closer. The amplification of the relative motion will thus be $(1 - 2\widetilde{K})/\chi_0$ which diverges when $\chi_0 \to 0$, which evidences the autoparametric resonance. The divergency of the travel time along the separatrix [26] implies the divergency of the time of parametric amplification in the limit $\chi_0 \to 0$. For a given $\widetilde{K}$ in the resonance tongue, the amplitude $\chi_{max} = 1 - 2\widetilde{K}$ that is eventually reached by the relative motion corresponds to the upper limit of the resonance tongue.

Apart from the parametric resonance *stricto sensu*, the phase portrait in the AP case evidences a parametric amplification when the relative motion amplitude is small (but not vanishingly small). Let us assume, *e.g.*, an initial value $\chi_0 = 0.1$. In the AP case (left plot of Fig. 1) the amplitude increases up to 0.65 whereas in the NR case (right plot of Fig. 1) the amplitude on this phase space trajectory is at most 0.15. The NR case is thus qualitatively different from the AP case in the whole phase portrait.

A common feature of both phase portraits is the periodic behavior of the eigenmodes amplitudes. The energy is given to the relative motion by the center of mass motion for $-\pi < \theta < 0$, and restituted to the center of mass motion in the next half period, without any net energy transfer when averaged on the slow time scale. Formally, this corresponds to the fact that the amplitude equations (10) exhibits *two* constants of the motion, whereas the underlying system (6) has only *one* constant of the motion, its conserved energy.

B. Sliding dimer.

Let us now consider the case of the sliding dimer. We assume that the initial kinetic energy of the center of mass is much larger than the depth of a potential well, so that the dimer motion is basically a monotonous translation of the center of mass together with oscillations of the particles around their equilibrium distance a. This amounts to assuming a strong enough interaction between the particles, in such a way that they cannot be distant from more than one period of the external potential. More general motions are studied

numerically in a forthcoming paper [24].

Setting the same dimensionless variables as before, and expanding the interaction potential up to order four in the small quantity y, we get the dimensionless equations of motion

$$\begin{cases} \ddot{x} = -\sin x \cos y, \\ \ddot{y} = -K_2 y + K_3 y^2 - K_4 y^3 - \cos x \sin y. \end{cases} \tag{30}$$

where $K_2 = (U''_{int}/U_0)(a/2\pi)^2$, $K_3 = (U^{(3)}_{int}/2U_0)(a/2\pi)^3$ and $K_4 = (U^{(4)}_{int}/6U_0)(a/2\pi)^4$. Let us emphasize the contrast with the trapped dimer configuration. In this case, the autoparametric resonance happens for a soft bond, so that the harmonic approximation of the interaction potential is sufficient. For a sliding dimer, we will see that the autoparametric resonance requires a strong bond, and consistently nonlinear terms in the interaction potential expansion are to be taken into account. Note also that in order to describe a physically sounded intermolecular interaction we have taken into account the fact that any reasonable interaction potential such as the Lennard-Jones potential [20], or such as the Morse potential which rather well describes chemical bonds [25] is dissymmetric near its minimum which requires the cubic term proportional to K_3.

Let V_0 be the initial velocity of the center of mass, in dimensionless units. Introducing $\tau = V_0 t$, the previous equations now read

$$\begin{cases} \ddot{x} = -\dfrac{1}{V_0^2} \sin x \cos y, \\ \ddot{y} = -\dfrac{K_2}{V_0^2} y + \dfrac{K_3}{V_0^2} y^2 - \dfrac{K_4}{V_0^2} y^3 - \dfrac{1}{V_0^2} \cos x \sin y, \end{cases} \tag{31}$$

where from now on $\dot{x} \equiv \mathrm{d}x/\mathrm{d}\tau$.

In the sliding configuration, the kinetic energy of the center of mass is much larger than the depth of the potential, $8U_0/(m\hat{V}_0^2) \ll 1$ (where $\hat{V}_0$ is the velocity in SI units) which in dimensionless units means $1/V_0^2 \ll 1$. Since it is the center of mass motion $x(\tau)$ that sets the velocity, it cannot be considered as small. In contrast, we assume a small amplitude of the relative motion, $|y| \ll 1$. To sum-up, we introduce the following expansions,

$$\begin{cases} x(\tau) = X_0 + \epsilon X_1 + \epsilon^2 X_2 + \ldots, \\ y(\tau) = \epsilon Y_1 + \epsilon^2 Y_2 + \epsilon^3 Y_3 + \ldots, \end{cases} \tag{32}$$

$$\frac{\mathrm{d}}{\mathrm{d}\tau} = \frac{\partial}{\partial T_0} + \epsilon \frac{\partial}{\partial T_1} + \epsilon^2 \frac{\partial}{\partial T_2} \quad \Longrightarrow \quad \frac{\mathrm{d}^2}{\mathrm{d}\tau^2} = \frac{\partial^2}{\partial T_0^2} + 2\epsilon \frac{\partial^2}{\partial T_0 \partial T_1} + \epsilon^2 \left(2\frac{\partial^2}{\partial T_0 \partial T_2} + \frac{\partial^2}{\partial T_1^2} \right), \tag{33}$$

where $\epsilon^2 \equiv 1/V_0^2 = U_0/(m\hat{V}_0^2) \ll 1$. We describe the stiff spring by setting

$$\frac{K_2}{V_0^2} = \frac{1}{4} - \eta\epsilon^2, \qquad \frac{K_3}{V_0^2} = \kappa_3, \qquad \frac{K_4}{V_0^2} = \kappa_4, \tag{34}$$

where the parameters η, κ_3 and κ_4 are assumed to be of order $\mathcal{O}(\epsilon^0)$. The chosen expression of K_2 conveniently describes the main parametric resonance.

Taking into account all terms up to order ϵ^3, the system (31) is writen perturbatively as

$$\left[\frac{\partial^2}{\partial T_0^2} + 2\epsilon\frac{\partial^2}{\partial T_0 \partial T_1} + \epsilon^2\left(2\frac{\partial^2}{\partial T_0 \partial T_2} + \frac{\partial^2}{\partial T_1^2}\right)\right](X_0 + \epsilon X_1 + \epsilon^2 X_2) = \\ = -\epsilon^2 \sin(X_0 + \epsilon X_1 + \epsilon^2 X_2)\cos\left(\epsilon Y_1 + \epsilon^2 Y_2 + \epsilon^3 Y_3\right), \tag{35}$$

$$\left[\frac{\partial^2}{\partial T_0^2} + 2\epsilon\frac{\partial^2}{\partial T_0 \partial T_1} + \epsilon^2\left(2\frac{\partial^2}{\partial T_0 \partial T_2} + \frac{\partial^2}{\partial T_1^2}\right)\right](\epsilon Y_1 + \epsilon^2 Y_2 + \epsilon^3 Y_3) = \\ = -\left(\frac{1}{4} - \eta\epsilon^2\right)(\epsilon Y_1 + \epsilon^2 Y_2 + \epsilon^3 Y_3) + \kappa_3(\epsilon Y_1 + \epsilon^2 Y_2 + \epsilon^3 Y_3)^2 - \\ -\kappa_4(\epsilon Y_1 + \epsilon^2 Y_2 + \epsilon^3 Y_3)^3 - \epsilon^2\cos(X_0 + \epsilon X_1 + \epsilon^2 X_2)\sin\left(\epsilon Y_1 + \epsilon^2 Y_2 + \epsilon^3 Y_3\right). \tag{36}$$

In the previous section, both modes have oscillatory behavior and the use of the multiple scales expansion is well documented [22]. In this section, we take advantage of the versatility of the multiple scale method, since the motion of the center of mass is not oscillatory but basically a translation. The calculations are thus explained in more details than in the previous section.

Order $\mathcal{O}(\epsilon^0)$.

At this order, the only contribution comes from Eqn. (35), and is readily solved

$$\frac{\partial^2 X_0}{\partial T_0^2} = 0, \quad \frac{\partial X_0}{\partial T_0} = A_0(T_1, \ldots), \quad X_0 = A_0(T_1, \ldots)T_0. \tag{37}$$

The initial conditions will be used at the end of the calculation, and for now $A_0(T_1, \ldots)$ is an unknown function of the slow scales $T_1, T_2, \ldots$. Nevertheless, it is important to keep in mind that, because of the definition of the time scale τ, $A_0 = 1 + \ldots$, where the dots stand for a small correction that will be found later to be of order ϵ^2.

order $\mathcal{O}(\epsilon)$.

The relevant terms from Eqn. (35) reads

$$\frac{\partial^2 X_1}{\partial T_0^2} = -2\frac{\partial^2 X_0}{\partial T_0 \partial T_1} = -2\frac{\partial A_0}{\partial T_1}. \tag{38}$$

To get a consistent expansion, the term X_1 should not increase faster with T_0 than X_0, which requires $\partial A_0/\partial T_1 = 0$ so that $A_0(T_2, \ldots)$. Then we take without loss of generality $X_1 = 0$ since the relevant initial condition on $x(t)$ may be set on X_0.

The term of order $\mathcal{O}(\epsilon)$ that comes from (36), reads

$$\frac{\partial^2 Y_1}{\partial T_0^2} + \frac{1}{4} Y_1 = 0, \quad Y_1 = B(T_1) e^{iT_0/2} + \overline{B}(T_1) e^{-iT_0/2}. \tag{39}$$

Order $\mathcal{O}(\epsilon^2)$.

At this order, we get the second order correction for x, which reads

$$\frac{\partial^2 X_2}{\partial T_0^2} = -\sin X_0 - 2\frac{\partial^2 X_0}{\partial T_0 \partial T_2} = -\sin(A_0 T_0) - 2\frac{\partial A_0}{\partial T_2}. \tag{40}$$

As before, to get a consistent expansion, the term X_2 should not increase faster with T_0 than X_0, which requires $\partial A_0/\partial T_2 = 0$. Therefore, the solution at this order reads

$$X_0 = A_0(T_3) T_0, \quad X_2 = \frac{1}{A_0(T_3)^2} \sin[A_0(T_3) T_0]. \tag{41}$$

The second order correction X_2 is thus independent on T_2 and T_1, which will be used later.

The term of order $\mathcal{O}(\epsilon^2)$ that comes from (36), reads

$$\frac{\partial^2 Y_2}{\partial T_0^2} + \frac{1}{4} Y_2 = -2\frac{\partial^2 Y_1}{\partial T_0 \partial T_1} + \kappa_3 Y_1^2 = -i\frac{\partial B}{\partial T_1} e^{iT_0/2} + \kappa_3 \left(B^2 e^{iT_0} + |B|^2 \right) + CC, \tag{42}$$

where "CC" means "complex conjugate". The resonant term must vanish, therefore $\partial B/\partial T_1 = 0$, and we get at this order

$$Y_2 = 8\kappa_3 |B(T_2)|^2 - \frac{4\kappa_3}{3} B(T_2)^2 e^{iT_0} - \frac{4\kappa_3}{3} \overline{B}(T_2)^2 e^{-iT_0}. \tag{43}$$

order $\mathcal{O}(\epsilon^3)$.

These terms occur in the relative motion equation (36), which reads

$$\frac{\partial^2 Y_3}{\partial T_0^2} + \frac{1}{4} Y_3 = -2\frac{\partial^2 Y_1}{\partial T_0 \partial T_2} + \eta Y_1 + 2\kappa_3 Y_1 Y_2 - \kappa_4 Y_1^3 - Y_1 \cos X_0 \tag{44}$$

To obtain the required amplitude equation for the relative motion, we only need the calculation of the secular term in the right hand member. It reads

$$\frac{\partial^2 Y_3}{\partial T_0^2} + \frac{1}{4} Y_3 = e^{iT_0/2} \left[-i\frac{\partial B}{\partial T_2} + \eta B - \left(3\kappa_4 - \frac{40\kappa_3^2}{3} \right) B^2 \overline{B} - \frac{\overline{B}}{2} e^{i(A_0 - 1)T_0} \right] + CC + NST \tag{45}$$

where NST means *non secular terms*. The last secular term comes from the coupling between the center of mass and relative motions. It is emphasized as the boxed term in

$$2Y_1 \cos X_0 = \left(Be^{iT_0/2} + \overline{B}e^{-iT_0/2}\right)\left(e^{iA_0T_0} + e^{-iA_0T_0}\right) = \\ = Be^{i\left(A_0+\frac{1}{2}\right)T_0} + \boxed{\overline{B}e^{i\left(A_0-\frac{1}{2}\right)T_0}} + Be^{-i\left(A_0-\frac{1}{2}\right)T_0} + \overline{B}e^{-i\left(A_0+\frac{1}{2}\right)T_0}.$$

The term in the box is indeed a secular term, because of the initial condition on the center of mass motion. From the center of mass motion at order ϵ^2, given by Eqn. (41), we must have

$$x(\tau) = A_0\tau + \frac{\epsilon^2}{A_0^2}\sin A_0\tau \quad \Longrightarrow \quad \frac{\mathrm{d}x}{\mathrm{d}\tau} = A_0 + \frac{\epsilon^2}{A_0}\cos A_0\tau.$$

In the variable τ, the initial velocity is unity, so that

$$\left.\frac{\mathrm{d}x}{\mathrm{d}\tau}\right|_{\tau=0} = A_0 + \frac{\epsilon^2}{A_0} = 1 \quad \Longrightarrow \quad A_0 = 1 - \epsilon^2 + \mathcal{O}(\epsilon^4).$$

Injecting this expression for A_0 in the secular term of Eqn. (45), we get the relevant amplitude equation for the relative motion as the solvability condition

$$\frac{\partial B}{\partial T_2} = -i\eta B + i\kappa B^2\overline{B} + i\frac{\overline{B}}{2}e^{-iT_2}, \quad \kappa \equiv 3\kappa_4 - \frac{40\kappa_3^2}{3}. \tag{46}$$

Setting $B = e^{-iT_2/2}D$, we recover the autonomous amplitude equation for the parametric instability,

$$\frac{\partial D}{\partial T_2} = i\left(\frac{1}{2} - \eta\right)D + i\kappa|D|^2D + i\frac{\overline{D}}{2}. \tag{47}$$

which is the same as Eqn. (12), apart from small changes in the notations. Note that the sign of κ is not relevant, since we can take the complex conjugate of this equation as well [4]. The condition of parametric amplification of the relative motion now reads

$$0 \leqslant \eta \leqslant 1. \tag{48}$$

III. DIMER IN A PERIODIC POTENTIAL : NUMERICAL SIMULATIONS.

In this section, we compare the analytic description of the previous section to direct numerical simulations of the actual dynamical system (6). For the comparison to make sense, the initial conditions for the numerical integration of the equations of motion have to be consistent with the approximations of the previous section. Therefore, we consider the cases of the dimer trapped in a well and of the sliding dimer separately.

A. Dimer in a well

For this configuration to takes place, a necessary condition is that the initial energy of the dimer should be less than the depth of the potential well. In the simulations, we take as initial conditions $x = 0$, $y = 0$ and non vanishing velocities. Since we choose the external potential energy as the energy scale, the relevant dimensionless parameter is

$$\epsilon^2 \equiv \left. \frac{m\,(\dot{x}_1^2 + \dot{x}_2^2)}{8U_0} \right|_{(t=0)} = \frac{\dot{x}_0^2 + \dot{y}_0^2}{4}, \tag{49}$$

and we assume $|\epsilon| \ll 1$ for the sake of comparison with the calculations of Sec. II A.

The main analytical result of Sec. II A are the coupled amplitude equations (10), whose solutions are fully described by the phase portraits displayed in Fig. 1. The dynamics of the eigenmodes is given by

$$\begin{cases} x(t) = 2\epsilon a \cos(t + \phi) = 2\epsilon a(\cos t \cos\phi - \sin t \sin\phi), \\ y(t) = 2\epsilon b \cos(t + \psi) = 2\epsilon b(\cos t \cos\psi - \sin t \sin\psi), \end{cases} \tag{50}$$

where the slowly varying amplitudes a and b are given by Eqn. (18) and where the slowly varying phases ϕ and ψ are given by Eqn. (15). The direct numerical simulations of the system (6) give $x(t)$ and $y(t)$ as rough numerical data, from which we have to extract the slowly varying amplitudes and phases. Once this is done, there remains no free parameter to undertake the comparison between the simulations and the multiple scale analysis.

An example of the signals $x(t)$ and $y(t)$ is displayed in Fig. 3, for initial conditions that are consistent with a small value of ϵ. The time evolution of both signals obviously validates the assumption of a slow variation of the amplitudes, with characteristic period much larger than 2π which is the quick time period. To calculate the amplitudes from the raw simulations data, we extract the local maxima, and then we build from these set an interpolation function in order to get a smooth function for the amplitude. Doing this, we get the slowly varying function

$$\chi(t) = \frac{b^2(t)}{a^2(t) + b^2(t)}. \tag{51}$$

To get the slowly varying phases, we multiply the raw numerical data by either $\cos t$ or $\sin t$, and take the average on the fast time variable. For example, we numerically integrate the simulations data to calculate

$$\langle X_C \rangle \equiv \frac{1}{2\pi} \int_0^{2\pi} x(t) \cos t \mathrm{d}t = \epsilon a \cos\phi, \tag{52}$$

since the slowly varying functions a and ϕ may be considered as constant for the integration. Since we already know the amplitude a as a (slow) function of time, we thus get $\cos\phi$. Replacing $\cos t$ by $\sin t$ in (52), we get $\sin\phi$ and doing the same work on $y(t)$ we get $\cos\psi$ and $\sin\psi$ as (slow) functions of time. Then we define complex variables $Z_\phi = \cos\phi + i\sin\phi$ and $Z_\psi = \cos\psi + i\sin\psi$, so that the variable θ is obtained as

$$\theta = \mathrm{Arg}\left(Z_\psi^2 / Z_\phi^2\right). \tag{53}$$

The numerical algorithms that calculate an angle as the argument of a complex number are the less sensitive to noise, which justifies their use.

This data analysis allows a direct comparison between the the phase space trajectories calculated from direct numerical simulations of the system (6) and the phase space trajectories provided by the multiple scale analysis, Eqn. (28). This is done in the upper plot of Fig. 2, for a dimensionless stiffness in the parametrically unstable tongue, $\widetilde{K} = 0.158$, and for initial conditions such that $\epsilon = 0.224$. Our data evidence an excellent agreement between the multiple scale analysis and the numerical data. In the bottom plot of Fig. 2, we compare the slow modulation period measured from direct numerical simulations (open circles) to a calculation derived from Eqn. (25) (crosses), for every phase space trajectories. This period is either the duration of one loop of a closed trajectory, or the travel time from $-\pi$ to π for an open trajectory. Here again, the numerical data are in excellent agreement with the multiple scale analysis. The period is an increasing function of the maximum amplitude χ_{max} for closed trajectories and a decreasing function of χ_{max} for open trajectories, since it diverges on the separatrix [26].

In Fig. 3 we plot the normal modes $x(t)$ and $y(t)$ as a function of time from a direct numerical integration of the system (6) and compare them to a numerical integration of the amplitude equations (19). We see that the amplitude equations accurately predict the slow modulation of the normal modes, without any fitting parameter. Moreover, we display zooms on both oscillatory modes in order to make the physical significance of the phase difference θ clearer. Initially, this phase difference vanishes. For an open trajectory in phase space (upper plot of Fig. 3, see Fig. 2 for the relevant phase trajectory) when the amplitude of $x(t)$ is maximal the amplitude of $y(t)$ is minimal and the two signals are in quadrature ($\theta/2 = \pi/2$). For a closed trajectory (bottom plot of Fig. 3, see Fig. 2 for the relevant phase trajectory) the phase difference is clearly less than $\pi/2$. This illustrates the link between

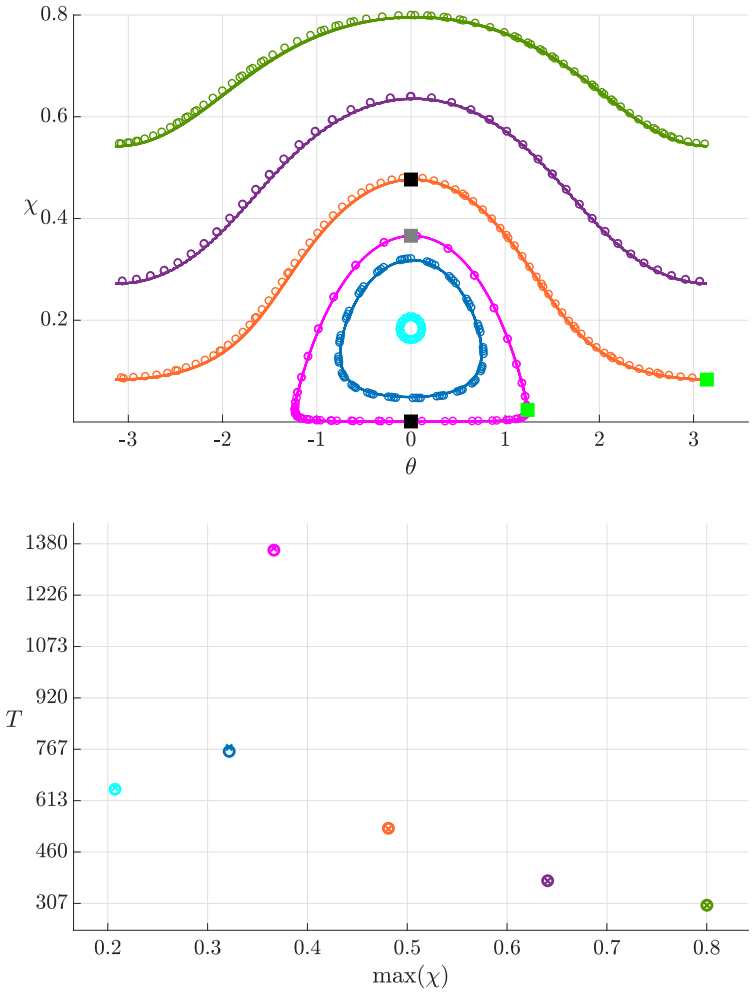

FIG. 2. (Color online). Top : Phase trajectories (θ, χ) from Eqn. (26) (dotted lines) and from numerical integration of (6) (solid lines) for $\widetilde{K} = 0.158$ and $\epsilon = 0.224$. The initial phase is $\theta_0 = 0$ in all simulations. The initial values χ_0 are : $\chi_0 = 0.8$ ($J = 0.013$), $\chi_0 = 0.64$ ($J = -0.047$), $\chi_0 = 0.48$ ($J = -0.082$), $\chi_0 = 0.32$ ($J = -0.091$), $\chi_0 = 0.16$ ($J = -0.075$), $\chi_0 = 0.001$ ($J = -0.034$). The filled squares correspond to the zooms in Fig. 3. Bottom : Slow oscillations period T (dimensionless) as a function of the maximum value of χ on the corresponding phase trajectory. Open circles from numerical integration of (6), crosses from Eqn. (26) (same color code as in the top plot).

the phase difference θ and the time evolution of $x(t)$ and $y(t)$.

It is clear that the actual dynamics of the dimer in an external potential well, obtained from direct numerical simulation of (6), is in excellent agreement with the multiple scale analysis of Sec. II A, whithout any fitting parameter. This is evidenced for $\epsilon = 0.224$, which is indeed not much smaller than unity. In a forthcoming paper [24] we extend our numerical

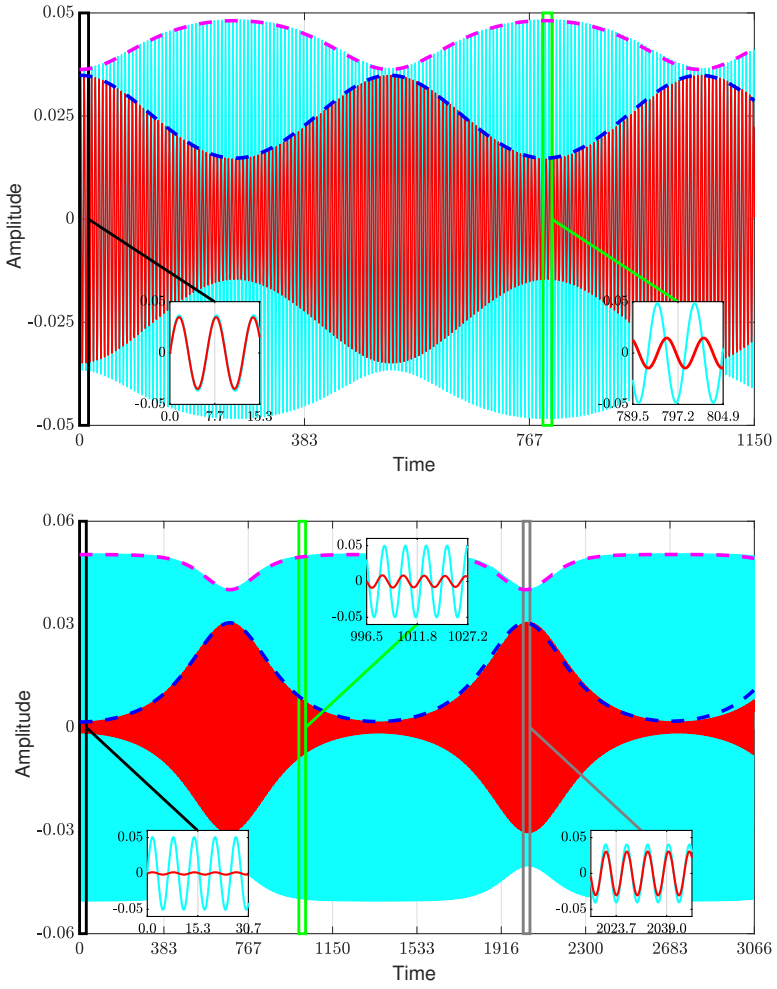

FIG. 3. (Color online). Plot of dimensionless amplitudes $x(t)$ (solid cyan lines) and $y(t)$ (solid red lines) as functions of the dimensionless time, from a numerical integration of (6) for $\widetilde{K} = 0.158$ and $\epsilon = 0.224$. The dashed lines are the slowly varying amplitudes of $x(t)$ (magenta) and $y(t)$ (blue), from a numerical integration of the amplitude equations (19), with initial phase $\theta_0 = 0$. The insets are zooms that correspond to the filled squares in Fig. 2. Upper plot : $\chi_0 = 0.52$ ($J = -0.082$), open trajectory in Fig. 2. The right hand zoom evidences that $x(t)$ and $y(t)$ are in quadrature, $\theta = \pi$. Bottom plot : $\chi_0 = 0.999$ ($J = -0.034$), closed trajectory in Fig. 2. The center zoom evidences a phase difference between x and y that is less than $\pi/2$. Note also the abcissae ranges.

simulations to larger values of ϵ. The agreement between the simulations and the multiple scale analysis is numerically excellent up to $\epsilon \approx 0.5$, and remains qualitatively correct up to the limit of trapped dimer, $\epsilon \leqslant 1$. The only strict condition is that of commensurability between the dimer and the external periodic potential. The motions where a particle may

jump to the next well are discussed in Ref. [24].

B. Sliding dimer

The analytic description of the dimer motion in the sliding configuration is expressed by the normal form (47) for the parametric amplification of a nonlinear oscillator without dissipation. It assumes that the initial velocity of the center of mass is such that the kinetic energy is much larger than the external potential well. As in Sec. II B, it is convenient to define $\tau = V_0 t$ and to set $\epsilon \equiv 1/V_0^2 \ll 1$. The actual system that describes the dimer motion, which is solved numerically, is thus the system (31). For the sake of comparison with the theoretical analysis, the initial conditions in the simulations of the system (31) are $x(t=0) = 0$, which only set the axis origin, $\dot{x}(t=0) = 1$ by definition of the time unit, $y(t=0) = y_0 \ll 1$ to put the focus on the autoparametric resonance, and $\dot{y}(t=0) = 0$. This exact numerical solution is then compared to the approximation provided by the multiscale analysis which gives the slowly varying amplitude of $y(t)$ as $2\epsilon|D|(t)$, where $D(t)$ is the numerical solution of Eqn. (47) with initial conditions $D(t=0) = y_0/(2\epsilon)$ (choosing a vanishing initial phase).

The sliding motion of the center of mass may induce a parametric amplification of the particles relative motion. This parametric amplification in the sliding regime only happens when the interaction is strong enough for the constants κ_i to be of the same order as the dimensionless kinetic energy V_0^2, as explained in (34). The condition for parametric excitation of the relative motion by the center of mass motion is given by (48). This behavior is illustrated in Fig. 4, in which we show the relative motion $y(t)$ as a function of time for several values of the shift η from the main parametric resonance. The numerical solution of the full system (31) evidences that the width of the resonance tongue in the vicinity of $K_2/V_0^2 = 1/4$ scales as ϵ^2, as expected from our theoretical analysis. In the center plot of Fig. 4 the value $\eta = 1/2$ is inside the parametric resonance tongue, and the relative motion $y(t)$ as a function of time exhibits the expected parametric resonance, with an amplitude amplification by a factor 100. In the left and right plots of Fig. 4 the values of η are outside the parametric resonance tongue, and consistently the relative motion $y(t)$ as a function of time exhibits no parametric resonance but low amplitude nonlinear beatings.

In Fig. 5, we compare the exact solution, given by the numerical integration of (31) to

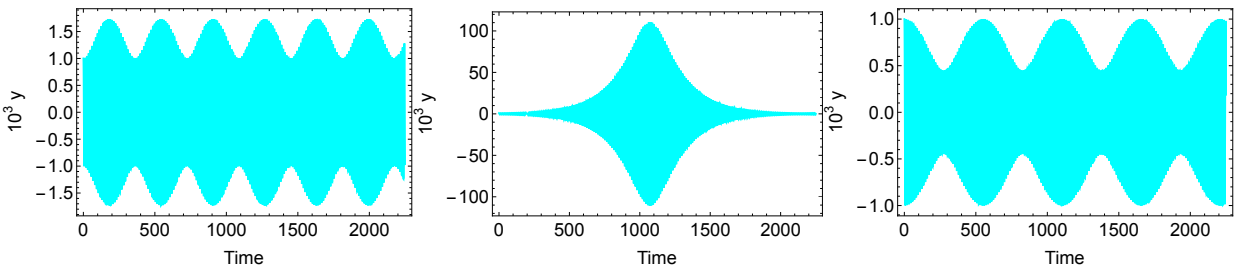

FIG. 4. (Color online). Plot of the dimensionless amplitude $10^3 y$ of the relative motion as a function of the dimensionless time from a numerical integration of the system (31). The relevant parameters are $\kappa = 1$, , $\kappa_4 = 1$, and $\epsilon = 0.1$. The initial conditions for the numerical integration are $x(0) = 0$, $\dot{x}(0) = 1$, $y(0) = 0.001$ and $\dot{y}(0) = 0$. From left to right the spring constant $1/4 - \epsilon^2\eta$ is 0.2375 ($\eta = 1.25$), 0.2450 ($\eta = 0.5$) and 0.2550 ($\eta = -0.5$). As expected, the relative motion inside the parametric resonance tongue (48) (center plot) is markedly different from the others which are outside the resonance tongue. We do not display the center of mass motion since it is in all cases basically a straight line of unit slope.

the predictions of the amplitude equation (47), for increasing values of the small parameter ϵ (from top to bottom). We see that the time evolution of the relative motion amplitude is indeed very well predicted by the asymptotic analysis, and the smaller ϵ the better. The maximum amplitude of the relative motion scales as ϵ, and the characteristic time for the parametric amplification of the relative motion scales as ϵ^2 (see the time scales in the plots). The amplitude growth begins as an exponential, which evidences the parametric amplification. The ratio between the maximum amplitude y_M of the relative motion and its initial value $y(0)$ is 350, 100 and 200 from top to bottom, which evidences a huge amplification of the relative motion. Since the system (31) is conservative, the energy transfer between the sliding motion of the center of mass and the relative motion is periodic.

Let us add a final remark. In Fig. 5, we still see a small discrepancy between the theoretical analysis and the numerical solution of the actual system for $\epsilon = 0.1$. Therefore, the range of validity of the multiscale analysis is much smaller in the sliding dimer case than when the dimer is trapped in a well. This is discussed at length in the forthcoming paper [24], where we also discuss the loss of commensurability of the configurations, when the link between the two particles is weak enough for one particle to jump farther away from the other than a period of the potential.

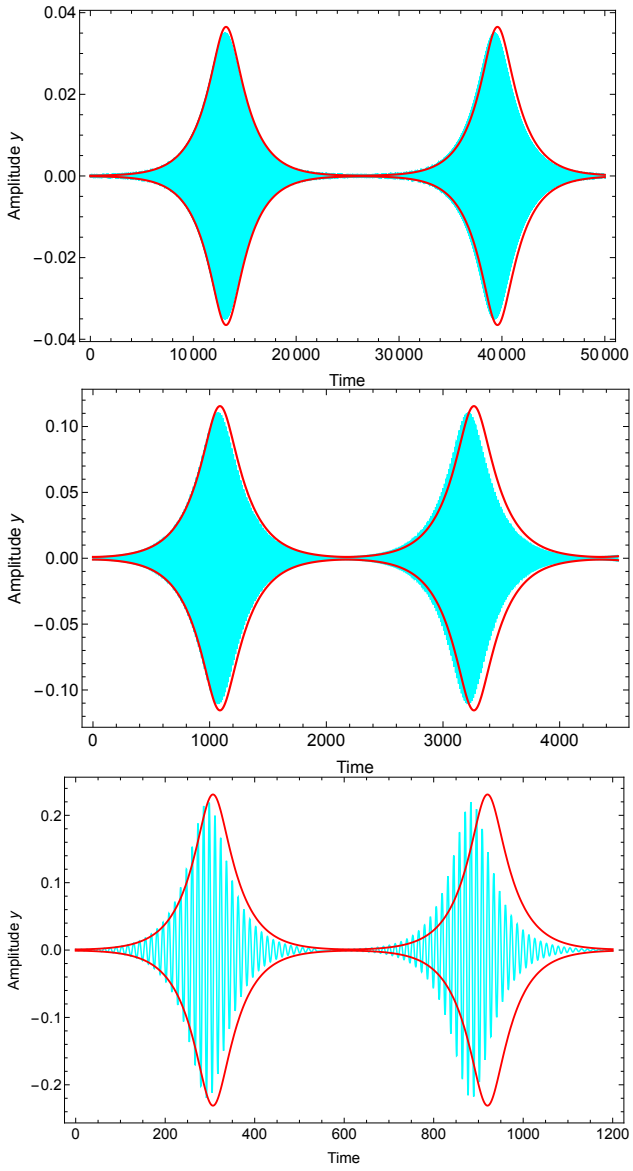

FIG. 5. (Color online). Cyan (light grey) solid line : Plot of the dimensionless amplitude y of the relative motion as a function of the dimensionless time from a numerical integration of the full system (31). Red (dark grey) solid line : Amplitude $R = |B|$ of the slow oscillations, from a numerical integration of the amplitude equation (47). The relevant parameters are $\kappa = 1$, $\kappa_4 = 1$ and $\eta = 1/2$, and from top to bottom $\epsilon = 0.032$, $\epsilon = 0.1$ and $\epsilon = 0.2$. The initial conditions for the numerical integration of (31) are $x(0) = 0$, $\dot{x}(0) = 1$, $\dot{y}(0) = 0$, and for the numerical integration of (47) we set $\phi(0) = Arg(B)|_{t=0} = 0$ and $R(0) = y(0)/(2\epsilon)$. Note that the choice $\dot{x}(0) = 1$ ensures that the time unit is the same in all plots. From top to bottom the initial condition for y is $y(0) = 0.0001$, $y(0) = 0.001$ and $y(0) = 0.001$ (same as before). In the first two plots the resolution is insufficient to distinguish the quick oscillations.

IV. CONCLUSION

A dimer in a periodic potential is a simple system with a complicated dynamics. It is conservative, but not integrable. Its motions are determined by its initial energy and the stiffness of the interaction between the particles. If the equilibrium length of the dimer is equal to the period of the potential, this commensurate configuration makes detailed calculations achievable in two limits.

In the first one, the initial energy and the interaction energy are small enough in comparison with the external potential energy barrier so that the dimer is trapped in a potential well. In this configuration, the center of mass motion may induce a parametric resonance of the relative motion for a soft bond of sufficiently low stiffness. The system comes down to coupled nonlinear oscillators that are easily addressed by a consistent multiple scale expansion. Moreover, the amplitude equations obtained with this analysis are found to be integrable, which allows a complete description of the dimer motions. When numerical simulations of the actual system are compared to the analytic description, this latter is found to describe accurately the motions of the dimer. It will be shown in a forthcoming paper [24] that the validity of our amplitude equations extends on much higher values of the small parameter (the ratio between the initial energy and the energy barrier) than expected. This system therefore exhibits autoparametric resonance between two oscillatory modes of a conservative system on a rather large parameter range.

The second configuration allowing a complete analytical description is when both the initial kinetic energy and the interaction energy are high enough in comparison with the external potential energy barrier for the dimer to slide along the external potential. The basic motion is the sliding of the dimer center of mass, that is coupled by the external potential to the relative motion of the particles. In this configuration, the center of mass motion induces a parametric resonance of the relative motion if there is a strong bond between the particles, so that we expand the interaction potential up to the fourth order. Taking advantage of the versatility of the multiple scales expansion, we show that the relevant amplitude equation is exactly that of the (cubic) nonlinear Mathieu equation, which is a paradigm of parametric amplification of a nonlinear oscillator. Since no external energy is provided to the system, this is another example of autoparametric behavior.

Apart from these two limiting cases, the system may exhibit complicated behaviors for

which the commensurability is lost, when the initial energy is high enough, and the interaction energy small enough for the particles to jump in non neighbouring potential wells. A description of such behaviors will be the subject of a forthcoming work [24]. Another extension of this work is to take into account a dissipative term, together with a non zero temperature.

Appendix A: Constants of motion for a trapped dimer

The equations (10) are Lagrange equations for the lagrangian

$$\mathcal{L} = i\left(A\dot{\overline{A}} - \overline{A}\dot{A}\right) + i\left(B\dot{\overline{B}} - \overline{B}\dot{B}\right) + \frac{|A|^4 + |B|^4}{4} + |A|^2|B|^2 - 2\widetilde{K}|B|^2 + \frac{B^2\overline{A}^2 + A^2\overline{B}^2}{4}, \quad \text{(A1)}$$

This lagrangian (A1) is obviously invariant under the transform

$$A \longrightarrow A' = Ae^{i\eta}, \quad \overline{A} \longrightarrow \overline{A}' = \overline{A}e^{-i\eta}, \quad B \longrightarrow B' = Be^{i\eta}, \quad \overline{B} \longrightarrow \overline{B}' = \overline{B}e^{-i\eta},$$

where η is a real constant phase. Assuming $|\eta| \ll 1$, we get the relevant infinitesimal transform, so that we deduce from Noether's theorem [27] the conserved quantity (16),

$$\frac{\partial\mathcal{L}}{\partial\dot{A}}(iA) + \frac{\partial\mathcal{L}}{\partial\dot{\overline{A}}}(-i\overline{A}) + \frac{\partial\mathcal{L}}{\partial\dot{B}}(iB) + \frac{\partial\mathcal{L}}{\partial\dot{\overline{B}}}(-i\overline{B}) = 2|A|^2 + 2|B|^2.$$

Another conserved quantity is due to the fact that the lagrangian (A1) has no explicit time dependence. The conserved quantity H reads

$$-H \equiv \dot{A}\frac{\partial\mathcal{L}}{\partial\dot{A}} + \dot{\overline{A}}\frac{\partial\mathcal{L}}{\partial\dot{\overline{A}}} + \dot{B}\frac{\partial\mathcal{L}}{\partial\dot{B}} + \dot{\overline{B}}\frac{\partial\mathcal{L}}{\partial\dot{\overline{B}}} - \mathcal{L},$$

so that

$$H = 2\widetilde{K}|B|^2 - |A|^2|B|^2 - \frac{|A|^4 + |B|^4}{4} - \frac{1}{4}\left(B^2\overline{A}^2 + A^2\overline{B}^2\right) \quad \text{(A2)}$$

There must be a relationship between H, N and the constant J, since only two of them may be independent. Indeed

$$H = 2\widetilde{K}(N - a^2) + \frac{a^4 + b^4}{4} - \underbrace{\left[a^2b^2 + \frac{a^4 + b^4}{2}\right]}_{=N^2/2} - \frac{1}{2}a^2b^2\cos\theta,$$

so that eventually

$$H - 2\widetilde{K}N + \frac{N^2}{2} = 2\left(\frac{a^4 + b^4}{8} - \widetilde{K}a^2 - \frac{1}{4}a^2b^2\cos\theta\right) = 2J.$$

Appendix B: About the constant N.

In all generality, the dimer motion depends on the initial conditions x_0, y_0, $\dot{x}_0$ et $\dot{y}_0$, in dimensional variables. For the analysis of Sec. II A to be relevant, the initial conditions must be such that

$$\frac{2\pi|x_0|}{a} \ll 1, \quad \frac{2\pi|y_0|}{a} \ll 1, \quad \sqrt{\frac{m}{U_0}}|\dot{x}_0| \ll 1, \quad \sqrt{\frac{m}{U_0}}|\dot{y}_0| \ll 1. \tag{B1}$$

Let us keep the tilde $\widetilde{\ }$ for the dimensionless variables, for the sake of clarity. Let us define

$$\widetilde{x}_0 \equiv \frac{2\pi x_0}{a}, \quad \widetilde{y}_0 \equiv \frac{2\pi y_0}{a}, \quad \dot{\widetilde{x}}_0 \equiv \sqrt{\frac{m}{U_0}}\dot{x}_0, \quad \dot{\widetilde{y}}_0 \equiv \sqrt{\frac{m}{U_0}}\dot{y}_0, \tag{B2}$$

where the dot means the derivation with respect to the dimensionless time $\widetilde{t}$. These dimensionless initial conditions are consistently of order ϵ. The amplitude equations (10) gives

$$\widetilde{x}\left(\widetilde{t}\right) = 2\epsilon a\cos\left(\widetilde{t}+\phi\right), \qquad \widetilde{y}\left(\widetilde{t}\right) = 2\epsilon b\cos\left(\widetilde{t}+\psi\right), \tag{B3}$$

where $a = \sqrt{N(1-\chi)}$ and $b = \sqrt{N\chi}$. The initial conditions for the dynamical variables χ, ϕ and ψ are given by Eqn. (B2), and reads

$$\begin{cases} \widetilde{x}_0 = 2\epsilon\sqrt{N(1-\chi_0)}\cos\phi_0, \\ \dot{\widetilde{x}}_0 = -2\epsilon\sqrt{N(1-\chi_0)}\sin\phi_0, \end{cases} \qquad \begin{cases} \widetilde{y}_0 = 2\epsilon\sqrt{N\chi_0}\cos\psi_0, \\ \dot{\widetilde{y}}_0 = -2\epsilon\sqrt{N\chi_0}\sin\psi_0. \end{cases} \tag{B4}$$

A simple manipulation gives

$$\begin{cases} \widetilde{x}_0^2 + \dot{\widetilde{x}}_0^2 = 4\epsilon^2 N(1-\chi_0), \\ \widetilde{y}_0^2 + \dot{\widetilde{y}}_0^2 = 4\epsilon^2 N\chi_0, \end{cases} \tag{B5}$$

therefore

$$\widetilde{x}_0^2 + \dot{\widetilde{x}}_0^2 + \widetilde{y}_0^2 + \dot{\widetilde{y}}_0^2 = 4\epsilon^2 N. \tag{B6}$$

If we define the small parameter ϵ as

$$\epsilon \equiv \frac{\sqrt{\widetilde{x}_0^2 + \dot{\widetilde{x}}_0^2 + \widetilde{y}_0^2 + \dot{\widetilde{y}}_0^2}}{2} \ll 1, \tag{B7}$$

we can take $N = 1$ in all generality. Physically, the small parameter is the ratio between the initial energy and the depth U_0 of the well.

We then get

$$\chi_0 \equiv \frac{\widetilde{y}_0^2 + \dot{\widetilde{y}}_0^2}{\widetilde{x}_0^2 + \dot{\widetilde{x}}_0^2 + \widetilde{y}_0^2 + \dot{\widetilde{y}}_0^2}, \tag{B8}$$

which is consistent with the requirement $0 < \chi_0 < 1$. Moreover, since we may write

$$\chi_0 \equiv \frac{\widetilde{y}_0^2 + \dot{\widetilde{y}}_0^2}{4\epsilon^2}, \qquad 1 - \chi_0 = \frac{\widetilde{x}_0^2 + \dot{\widetilde{x}}_0^2}{4\epsilon^2}, \tag{B9}$$

we see that injecting these expressions in the system (B4) we get consistent real values for the phases, since the relevant trigonometric functions range between -1 and 1.

---

[1] Elena Kartashova, *Nonlinear Resonance Analysis: Theory, Computation, Applications* (Cambridge University Press, 2010).

[2] L.D. Landau and E. Lifchitz, *Mécanique* (Mir Editions, Moscou, 1966).

[3] M. Mond, G. Cederbaum, P.B. Khan, and Y. Zarmi, "Stability analysis of the non-linear Mathieu equation," J. Sound Vibr. **167**, 77–89 (1993).

[4] S. Fauve, "Nonlinear dynamics of coupled oscillators," Ann. Phys. Fr. **19**, 691–714 (1994).

[5] Hideyuki Kidachi and Hiroshi Onogi, "Note on the stability of the nonlinear Mathieu equation," Prog. Theor. Phys. **98**, 755 (1997).

[6] R.S. Zounes and R.H. Rand, "Subharmonic resonance in the non-linear Mathieu equation," Int. J. Non-Lin. Mech. **37**, 43–73 (2002).

[7] Chaouqi Misbah, *Complex Dynamics and Morphogenesis* (Springer Verlag, Dordrecht, 2017).

[8] V.L. Safonov, M.E. McConney, and M.R. Page, "Simple hamiltonian approach to describe large-amplitude and high-order parametric resonances," Phys. Rev. E **100**, 040201(R) (2019).

[9] B. Denardo, J. Earwood, and V. Sazonova, "Parametric instability of two coupled nonlinear oscillators," Am. J. Phys. **67**, 187 (1999).

[10] R. Naz, I. Naem, and F.M. Mahomed, "First integrals for two linearly coupled nonlinear Duffing oscillators," Math. Prob. Eng. (2011), 10.1155/2011/831647.

[11] S. Sabarathinam, K. Thamilmaran, L. Borkowski, P. Perlikowski, P. Brzeski, A. Stefanski, and T. Kapitaniak, "Transient chaos in two coupled, dissipatively perturbed hamiltonian Duffing oscillators," Commun Nonlinear Sci Numer Simulat **18**, 3098 (2013).

[12] S. Lenci, "Exact solutions for coupled Duffing oscillators," Mech. Syst. Sig. Proc. **165**, 108299 (2022).

[13] S.V. Kuznetsov, "The motion of the elastic pendulum," R & C Dynamics **4**, 3 (1999).

[14] Peter Lynch and Conor Houghton, "Pulsation and precession of the resonant swinging spring," Physica D **190**, 38–62 (2004).

[15] M. A. Abramowicz, T. Bulik, M. Bursa, and W. Kluźniak, "Evidence for a 2:3 resonance in Sco X-1 kHz QPOs," A & A (2003).

[16] W. Kluźniak and M. A. Abramowicz, "Resonant oscillations of accretion flow and kHz QPOs," Astrophys. Space Sci. **300**, 143–148 (2005).

[17] J. Horak, "The autoparametric 3:2 resonance in conservative systems," Astron. Nachr. **326**, 824–829 (2005).

[18] J. Horak, *Oscillations and lightcurve patterns of accreting black holes*, Ph.D. thesis, Charles University in Prague (2005).

[19] A. S. Kovalev and A. I. Landau, "Dynamical chaos and low-temperature surface diffusion of small adatom clusters," J. Low Temp. Phys. **28**, 423 (2002).

[20] C. Fusco, A. Fasolino, and T. Janssen, "Nonlinear dynamics of dimers on periodic substrates," Eur. Phys. J. B **31**, 95 (2003).

[21] Marcin Minkowski and Magdalena A. Zaluska-Kotur, "Diffusion of Cu adatoms and dimers on Cu(111) and Ag(111) surfaces," Surface Science **642**, 22 (2015).

[22] Ali H. Nayfeh, *Perturbation methods* (John Wiley and sons, New York, 1973).

[23] In Refs. [4] and [7], the normal form takes into account a dissipative term proportional to the oscillator velocity, with a coefficient that for consistency scales as ϵ^2.

[24] Johann Maddi, Christophe Coste, and Michel Saint Jean, "In preparation," .

[25] R.J. Le Roy and R.D.E. Henderson, "A new potential function form incorporating extended long-range behaviour: application to ground-state Ca_2," Mol. Phys. **105**, 663 (2007).

[26] John H. Lowenstein, *Essentials of hamiltonian dynamics*, edited by Cambridge University Press (2012).

[27] Herbert Goldstein, *Classical Mechanics* (Addison-Wesley, 1980).